Navigation, Guidance and Control For the CICADA Expendable Micro Air Vehicle

Aaron D. Kahn *
Daniel J. Edwards †
US Naval Research Laboratory, Washington, DC 20375

The CICADA (Close-in Covert Autonomous Disposable Aircraft) is a new and novel micro air vehicle design based on a monolithic circuit-board/structure. The CICADA is a glider which once dropped from a host vehicle will automatically fly to a preprogrammed recovery waypoint. A key design goal for the guidance and control system was to enable the CICADA to recover from a wide range of initial launch conditions and altitudes. Recording temperature and wind profile data during the decent was also a design objective. This paper will describe the navigation, guidance, flight control, and environmental control developed for this simple yet capable aircraft. Flight test data will be presented showing the performance of the CICADA vehicle from a drop of over 29,000 feet in altitude.

I. Introduction

Unmanned aerial sensors (UAS) have typically been complex assemblies of the airframe, payload, and flight control system. In some missions, such as ground sensor emplacement, stand-in electronic warfare, or payload delivery, a low-cost system is desired. In these missions the vehicle is considered disposable. Working towards the goal of a low-cost, disposable UAS, the U.S. Naval Research Laboratory has developed the CICADA (Close-in Covert Autonomous Disposable Aircraft) vehicle for use as a small, disposable delivery platform. The CICADA is a simple glider, designed to deliver a payload to a preprogrammed location on the ground.[1] In order to make the CICADA vehicle practical for large-scale production, minimizing cost per vehicle was a primary goal. An innovative design aspect of the CICADA is the use of the flight control system circuit board as the primary structure of the vehicle. This design feature minimizes the assembly time by tightly integrating the flight control system and airframe eliminating the interconnect wiring typically found in traditional UAS design. Another cost saving element was the use of a minimal sensor suite for the navigation system.

Prior efforts have been made on the design of navigation and control system based on minimal sensor suites. Johnson et. al. designed a state estimation system around a single GPS receiver and plant model of the aircraft.[2] In this design the GPS receiver is used to update a state observer which is being driven using the aileron, elevator, and throttle commands from the controller. This technique tends to have poor disturbance rejection ability, as only the slow system states are directly observable via the GPS receiver. It also requires that the plant be statically stable. Other minimal systems have been developed which use thermopile sensors for horizon sensing[3].[4] All of these systems require prior calibration of the thermal sensors prior to flight, or the inclusion of additional vertical sensors for calibration. Thermal sensing systems are based on the assumption that the ground is warmer than the sky. This assumption can be violated if the vehicle is above cloud cover, where the thermal sensors' view of the ground is obscured. These system also suffer from drift over temperature due to differences in the temperature stability of the thermopile sensors.[5]

Due to the high dynamics expected at launch, and the unstable spiral mode of the CICADA air vehicle, the GPS-only approach as presented in Reference 2 is not viable. The thermopile systems as presented in References 3 and 4 looked promising, but as the CICADA will be launched from altitudes in excess of 30,000 feet the system would suffer from significant drift due to the large change in temperature. Also, there exists

*Senior Aerospace Engineer, AIAA Member
†Aerospace Engineer

Report Documentation Page

Form Approved
OMB No. 0704-0188

1. REPORT DATE	2. REPORT TYPE	3. DATES COVERED
2015		**00-00-2015 to 00-00-2015**

4. TITLE AND SUBTITLE	5a. CONTRACT NUMBER
Navigation, Guidance and Control For the CICADA Expendable Micro Air Vehicle	5b. GRANT NUMBER
	5c. PROGRAM ELEMENT NUMBER
6. AUTHOR(S)	5d. PROJECT NUMBER
	5e. TASK NUMBER
	5f. WORK UNIT NUMBER
7. PERFORMING ORGANIZATION NAME(S) AND ADDRESS(ES) **US Naval Research Laboratory,,Washington,,DC, 20375**	8. PERFORMING ORGANIZATION REPORT NUMBER
9. SPONSORING/MONITORING AGENCY NAME(S) AND ADDRESS(ES)	10. SPONSOR/MONITOR'S ACRONYM(S)
	11. SPONSOR/MONITOR'S REPORT NUMBER(S)

12. DISTRIBUTION/AVAILABILITY STATEMENT
Approved for public release; distribution unlimited

13. SUPPLEMENTARY NOTES

14. ABSTRACT

The CICADA (Close-in Covert Autonomous Disposable Aircraft) is a new and novel micro air vehicle design based on a monolithic circuit-board/structure. The CICADA is a glider which once dropped from a host vehicle will automatically fly to a preprogrammed recovery waypoint. A key design goal for the guidance and control system was to enable the CICADA to recover from a wide range of initial launch conditions and altitudes. Recording temperature and wind profile data during the decent was also a design objective. This paper will describe the navigation, guidance, flight control, and environmental control developed for this simple yet capable aircraft. Flight test data will be presented showing the performance of the CICADA vehicle from a drop of over 29,000 feet in altitude.

15. SUBJECT TERMS

16. SECURITY CLASSIFICATION OF:			17. LIMITATION OF ABSTRACT	18. NUMBER OF PAGES	19a. NAME OF RESPONSIBLE PERSON
a. REPORT	b. ABSTRACT	c. THIS PAGE			
unclassified	**unclassified**	**unclassified**	**Same as Report (SAR)**	**15**	

the possibility that the CICADA will be flying above the cloud base. To address the deficiencies of these attempts a fully inertial-based navigation system was designed. The CICADA navigation system design features a single GPS receiver, roll-axis rate gyroscope, and a yaw-axis rate gyroscope as the only flight control sensors. Additional environmental sensors were added to support operations at high altitude and provide additional atmospheric data for flight test.

This paper will describe the development of the guidance, navigation, and control system for the CICADA air vehicle. The CICADA vehicle design will be covered briefly in Section II. Section III will describe in detail the navigation system design. Section IV will cover the basic guidance law used to command the vehicle to a single waypoint, and then orbit around that location until impact with the ground. Section V will describe the vehicle control systems for both flight control and environmental control. Finally Section VI will illustrate the performance of the overall system with data from a drop of over 29,000 feet in altitude.

II. Vehicle Description

The CICADA vehicle was developed as a novel solution for the need of a low-cost, disposable aircraft. A novel design feature of the CICADA airframe is that the vehicle's main structure is also the avionics circuit board. This design feature drastically reduced overall assembly time by fully integrating all of the electronic components onto the one circuit board. The CICADA vehicle was designed be able to operate at altitudes of greater than 30,000 feet. This required some additional environmental controls to counter the effect of the extreme cold at these altitudes. A thin-film heater was designed into the system to warm the lithium-polymer batteries. A sintered nylon shell was designed to encase the bottom of the fuselage/circuit card. This cavity was then filled with 2-part foam to provide further thermal insulation, and to prevent condensation from developing on the electronic components. The CICADA vehicle and circuit card fuselage is shown in Figure 1a. The CICADA vehicle as flown in shown in Figure 1b. The wing of the CICADA is made from the same FR4 fiberglass sheet material which the fuselage/circuit board is made of. Lightning holes were cut into the wing, and covered with common packing tape. Pitch and roll control is provided by elevons at the trailing edge of the wing.

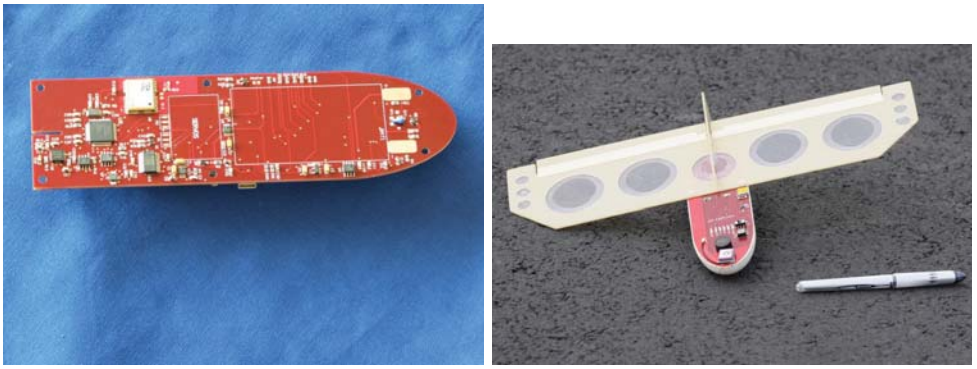

(a) CICADA main circuit board/fuselage (b) CICADA vehicle

Figure 1: CICADA vehicle and circuit board fuselage

Wing Span	14 in
Wing Area	52.5 in^2
Weight	7 oz
L/D	3
Trim Indicated Airspeed	49 ft/s

Table 1: CICADA vehicle parameters

The mission design goals for the flight control system were: 1) recover the vehicle from a deployment with unknown initial conditions; 2) be robust to manufacturing tolerance errors; 3) guide the vehicle to a pre-programmed waypoint location and orbit that location until impact with the ground; 4) record atmospheric

data during the decent; 5) provide thermal control for battery heating. The sensors chosen for primary flight control were a uBlox NEO-6 GPS receiver[6] and dual-axis rate gyroscope[7] measuring the roll-axis and yaw-axis angular rates. Power was provided by a pair of 800 mAh lithium-polymer cells connected in parallel. The flight computer was a LPC2138 ARM7 microcontroller running at a clock rate of 60 MHz.[8] Additional sensors were two temperature sensors, one for circuit board temperature and the other for battery temperature. In order to make recovery after landing easier, a small beeper was also designed into the system. The flight computer would activate the beeper upon crossing a threshold altitude during decent. A hall-effect sensor was included in the design to provide knowledge of when the CICADA vehicle was free of the host platform. While on the host platform, all integrator states are frozen and the elevon positions are fixed.

III. Navigation

The navigation system design for the CICADA was focused on providing a robust estimate of the roll attitude and vertical velocity of the vehicle. In addition, it was desired to estimate the wind field during the descent. As described, the only sensors designed into the flight control system were a single GPS receiver and a dual-axis rate gyroscope measuring body roll and yaw rate. Due to the large temperature range over which the vehicle was expected to operate, the navigation system was designed to mitigate the large biases expected in the rate sensors.

A. Roll Attitude Estimation

A complementary filter was designed for the estimation of roll attitude. The roll-rate sensor was used to provide the filter derivative, and the GPS track-rate was used as the measurement. In order to cancel the bias of the roll-rate sensor, the sensor output was passed through a washout filter.[9] The time constant of the washout filter in Equation 1 was set to 10 seconds.

$$\hat{p} = \frac{\tau s}{\tau s + 1} p \tag{1}$$

The roll attitude derivative was then computed assuming small pitch angles such that $\dot{\Phi} = \hat{p}$. The measurement for the complementary filter was derived using the coordinated turn assumption from the GPS ground track.[9] The GPS ground track information was back-differenced to derive track rate $\dot{\Psi}$. Equation 2 was then used to compute the measured roll attitude. The function atan2() is the 4-quadrant $\tan^{-1}()$ function.

$$\Phi_{meas} = \text{atan2}\left(\dot{\Psi} V_g, G\right) \tag{2}$$

The ground speed, V_g, was provided by the GPS sensor. The roll attitude estimate was updated using Equation 3 with gain $K_\Phi = 0.7$.

$$\Phi^+ = \Phi^- + K_\Phi \left(\Phi_{meas} - \Phi^-\right) \tag{3}$$

The measurement updates were performed at the GPS update rate of 4 Hz. If the GPS data was not valid then Φ_{meas} was set to 0 in Equation 3. This complementary filter proved to perform well for all flight conditions, and was robust to large launch disturbances. The use of the washout filter in Equation 1 proved to work well in countering biases in the roll-rate sensor without degradation to the roll estimate.

B. Vertical Velocity Estimation

Vertical velocity information is required by the flight path angle controller. It was found during testing that the GPS sensor's vertical velocity measurement was quite noisy when compared to the altitude measurement. The flight path angle controller is designed to automatically adjust the trim elevator setting of the elevons, and is therefore a "slow" process. An accurate measure of vertical velocity is required for this controller to function correctly. The vertical velocity estimator is based on a complementary filter using the altitude from the GPS receiver as the measurement. The derivative of vertical velocity, V_D, was assumed to be 0.

$$H = \int -V_D dt \tag{4}$$

The estimate of the altitude H and vertical velocity V_D is seeded with the GPS data when the GPS sensor data first becomes valid. The altitude estimate is then propagated using the estimated vertical velocity

in Equation 4. When a new GPS altitude measurement H_{meas} is available, the filter updates the vertical velocity estimate using Equation 5 with $K_H = 0.9$.

$$\begin{aligned} V_D^+ &= V_D^- + K_H \left(H - H_{meas}\right) && (5) \\ H &= H_{meas} && (6) \end{aligned}$$

It was found that no measurement update using the GPS vertical velocity measurement was needed, and in fact only added noise to the vertical velocity state.

C. True Airspeed Calculation

The guidance system and control system required the knowledge of the true airspeed of the vehicle. The flight control system has no air-data sensors, therefore the true airspeed of the vehicle was computed using the NASA standard atmosphere model.[10] The trim indicated airspeed of the vehicle was set as $IAS_0 = 49 ft/s$. This trim airspeed is maintained via the flight path angle controller. The true airspeed was then computed using Equation 7.

$$TAS = IAS_0 \sqrt{\frac{\rho_0}{\rho\left(H\right)}} \tag{7}$$

The value ρ_0 is the density at sea-level and the function $\rho(H)$ returns the density of the air based on the standard atmosphere model at the given altitude H.

D. Wind Estimation

While not required for flight control or guidance, it was desired to estimate the wind speed and direction during the decent phase of flight. The wind estimation algorithm is based on the assumption that the vehicle's airspeed does not change quickly, which is valid for the CICADA. An extended Kalman filter was implemented to estimate the winds. The states of the filter are true airspeed, north wind component, and east wind component, as shown in Equation 8. All states were assumed to be Gaussian random constants such that $\dot{\hat{X}} = 0$.

$$\hat{X} = \begin{bmatrix} \hat{V}_{true} & \hat{W}_n & \hat{W}_e \end{bmatrix}^T \tag{8}$$

The process noise matrix for the filter was chosen as $Q = Diag(0.001, 0.001, 0.001)$. The covariance matrix was initialized as $P = Diag(0.4, 0.1, 0.1)$. As the system model is 0, the covariance matrix derivative is simply $\dot{P} = Q$. The measurement equation for the wind estimator is based on the relationship

$$\bar{V}_g = \bar{V}_a + \bar{V}_w \tag{9}$$

where $\bar{V}_g$ is the inertial velocity vector over the ground, $\bar{V}_a$ is the true airspeed inertial velocity vector, and $\bar{V}_w$ is the inertial wind vector. Equation 9 is rewritten as Equation 10 to isolate the airspeed velocity vector. The airspeed vector is converted to a scalar value by taking the vector norm of both sides of Equation 10.

$$\begin{aligned} \bar{V}_a &= \bar{V}_g - \bar{V}_w && (10) \\ \left|\bar{V}_a\right| &= \left|\bar{V}_g - \bar{V}_w\right| && (11) \end{aligned}$$

$$0 = \left|\bar{V}_g - \bar{V}_w\right| - \left|\bar{V}_a\right| \tag{12}$$

Equation 12 can be written based on the state estimates as

$$\begin{aligned} N_{err} &= \bar{V}_{g_n} - \hat{W}_n \\ E_{err} &= \bar{V}_{g_e} - \hat{W}_e \\ \epsilon &= \sqrt{N_{err}^2 + E_{err}^2} - \hat{V}_{true} && (13) \end{aligned}$$

where $\bar{V}_g$ is the inertial ground speed vector available from the GPS sensor.

Using the measurement Equation 13 the extended Kalman filter measurement can be computed using Equations 14-17.[11]

$$\frac{\partial \hat{V}_{true}}{\partial \epsilon} = -1 \qquad \frac{\partial \hat{W}_n}{\partial \epsilon} = \frac{-N_{err}}{\sqrt{N_{err}^2 + E_{err}^2}} \qquad \frac{\partial \hat{W}_e}{\partial \epsilon} = \frac{-E_{err}}{\sqrt{N_{err}^2 + E_{err}^2}}$$

$$C = \begin{bmatrix} \frac{\partial \hat{V}_{true}}{\partial \epsilon} & \frac{\partial \hat{W}_n}{\partial \epsilon} & \frac{\partial \hat{W}_e}{\partial \epsilon} \end{bmatrix} \tag{14}$$

$$K = PC^T \left(CPC^T + R\right)^{-1} \tag{15}$$

$$\hat{X}^+ = \hat{X}^- + K\left(0 - \epsilon\right) \tag{16}$$

$$P^+ = P^- - KCP^- \tag{17}$$

This measurement update is attempting to drive $\epsilon = 0$ based on the derivation of Equation 12. It is noted that the wind states are only observable during turning flight. It is because of this limitation that the true airspeed estimate was not used in the guidance and control system.

IV. Guidance

A basic guidance system was designed to command the vehicle towards a preprogrammed waypoint and then to orbit the waypoint until impact with the ground. The guidance system was designed as a finite state machine with three operating modes. The first mode is used when the vehicle is far away from the waypoint and is to track towards it. The second mode is for orbiting the waypoint. The third mode is to handle the case when the GPS receiver is not providing valid data. The guidance equations were derived assuming a 2-D flat plane tangent to the Earth's surface at the location of the waypoint. As the CICADA does not know the altitude of the waypoint, nor the altitude of the ground, no vertical guidance is required. The output of the guidance system is a roll attitude command.

The guidance calculations are done in North-East plane, relative to the waypoint location. As the GPS receiver is providing position data in latitude and longitude, a conversion is required to compute the position relative to the waypoint location. The waypoint position is given as $P = [\lambda\ \mu]$ with λ as latitude and μ as longitude. Conversion factors C_λ and C_μ are computed in Equations 18 and 19 using the waypoint latitude λ.

$$e = 0.0818191909289$$

$$a = 6378137.0\ m$$

$$C_\lambda = \frac{a\left(1 - e^2\right)}{\left(1 - e^2 \sin^2(\lambda)\right)^{3/2}}\ m/rad \tag{18}$$

$$C_\mu = \frac{a\cos(\lambda)}{\sqrt{1 - e^2 \sin^2(\lambda)}}\ m/rad \tag{19}$$

The position of the vehicle from the waypoint in the North-East plane can then be computed.

$$P_n = C_\lambda\left(\lambda - \lambda_{gps}\right) \tag{20}$$

$$P_e = C_\mu\left(\mu - \mu_{gps}\right) \tag{21}$$

$$\Psi = \text{atan2}\left(P_e, P_n\right) \tag{22}$$

$$D = \sqrt{P_n^2 + P_e^2} \tag{23}$$

The bearing angle Ψ, and range D, are computed in Equations 22 and 23 using the north and east positions, P_n and P_e.

A. Guidance Modes

The modes of the guidance system are defined by the range of the vehicle to the target waypoint when GPS data is valid. Figure 2a shows the various ranges which define the switch points for these modes. In Figure 2a, R is defined as the desired orbit radius. The state logic is shown in Figure 2b.

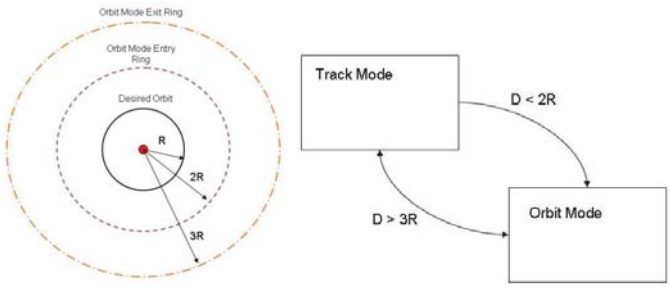

(a) Guidance mode switch points (b) Guidance logic states

Figure 2: Guidance system mode logic

At high altitude, the CICADA will be flying faster than at low altitude. Thus, at a given bank angle, the orbital radius is larger than at sea-level. In order to allow the orbital guidance controller enough maneuver margin, the orbit radius is calculated as a function of altitude. Using the value TAS from Equation 7 and 70-percent of the maximum bank angle command, $\bar{\Phi}$, the minimum orbit radius achievable is calculated using Equation 24.

$$R_{min} = \frac{TAS^2}{G\tan(0.7\bar{\Phi})} \tag{24}$$

The orbit radius used in the guidance system is then $R = \max(R_{des}, R_{min})$, where R_{des} is the desired orbit radius provided and R_{min} is computed from Equations 24.

1. Track Mode

If the vehicle is sufficiently far away from the waypoint, the goal of the guidance system is to direct the vehicle towards the waypoint. In this mode, it is assumed that the vehicle is capable of always moving in the direction of the waypoint. The track controller is implemented as a type of pursuit guidance, where the error between the GPS ground track and the bearing angle is driven to 0. The track controller is shown in Equation 25.

$$\begin{aligned} e &= \text{modangle}\left(\Psi - \Psi_{gps}\right) \\ \dot{\Psi} &= K_t\left(e + x_t\right) \qquad (25) \\ x_t &= \int K_{i_t} e \; dt \qquad (26) \end{aligned}$$

The function modangle(x) will wrap and angle such that it is between $-\pi$ and π. The turn-rate command $\dot{\Psi}$ is then used to compute the commanded bank angle Φ_c.

$$\begin{aligned} \Phi_{des} &= \text{atan2}\left(\dot{\Psi} V_g, G\right) \qquad (27) \\ \Phi_{cmd} &= \text{sat}\left(\Phi_{des}, \pm\bar{\Phi}\right) \qquad (28) \end{aligned}$$

The desired bank angle result of Equation 27 is limited to the maximum allowable bank angle in Equation 28. If $\Phi_{des} = \Phi_{cmd}$ the integrator state is propagated using Equation 26.

2. Orbit Mode

The orbit mode controller will cause the vehicle to fly a clockwise orbit as viewed from above around the commanded waypoint. The target orbit radius, R was already defined above. Figure 3 illustrates the basic orbit control law.

$$\begin{aligned} R_e &= D - R \qquad (29) \\ \Delta\Psi &= \text{sat}\left(K_o \; R_e, \pm 0.52\right) \qquad (30) \\ \Psi_0 &= \text{modangle}\left(\Psi - \frac{\pi}{2}\right) \qquad (31) \\ \Psi_{cmd} &= \text{modangle}\left(\Delta\Psi + \Psi_0\right) \qquad (32) \end{aligned}$$

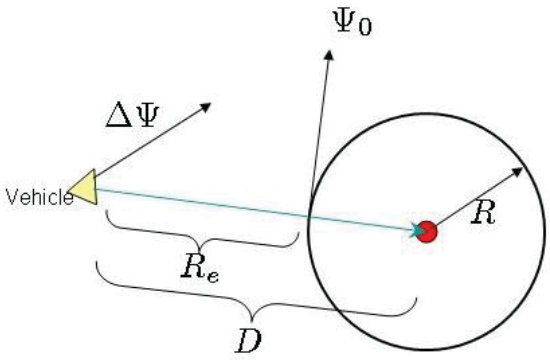

Figure 3: Orbit controller

The desired track to follow is computed in Equation 32. This command is made of two parts. The first is the nominal track, which is just the bearing perpendicular to the bearing to the waypoint. The second part is the offset as a function of the error in range to the target orbit radius. The orbit gain K_o defines how much to adjust the nominal track so the vehicle will fly at the given radius. If only this was used in the orbit controller, the vehicle would always fly outside of the orbit. To provide the required lead to the controller, a trim track-rate command is generated using Equation 33.

$$\Delta\dot{\Psi} = \frac{V_g}{\max(D, R)} \tag{33}$$

$$\dot{\Psi} = K_t \ \text{modangle}\left(\Psi_{cmd} - \Psi_{gps}\right) + \Delta\dot{\Psi} \tag{34}$$

Using the result of Equation 34 as the input to Equation 27, the final roll command from the orbit guidance controller is computed.

3. No GPS Mode

In the event of total GPS sensor failure, the guidance system is not capable of calculating a nominal roll attitude command. In this mode, the roll command Φ_c is set to 0.

V. Control

The CICACA flight control system is composed of three control loops. Two of the loops are dedicated to flight control, while the third loop is for the control of the battery temperature. The flight control loops are the roll attitude and flight path angle control loops. These are implemented as traditional linear PID controllers with integrator anti-windup protection. The thermal controller was implemented as a basic thermostatic loop with hysteresis, and additional logic which takes into account battery voltage.

A. Roll Control

Roll control of the vehicle is provided by differential deflection of the elevon control surfaces, which will be called δ_{ail}. The roll controller uses the estimated roll attitude state and washed out roll-rate from the navigation system. The roll-attitude command is provided by the guidance system.

$$e = \text{modangle}\left(\Phi_c - \Phi\right)$$

$$\delta_{ail_{des}} = R_{p_{ail}}\left(e + x_\phi\right) + R_{d_{ail}}\hat{p} \tag{35}$$

$$x_\phi = \int R_{i_{ail}} e \ dt \tag{36}$$

The desired aileron deflection is limited to $\delta_{ail} = \text{sat}(\delta_{ail_{des}}, \pm\bar{\delta}_{ail})$ where $\bar{\delta}_{ail}$ is the maximum differential deflection. If $\delta_{ail_{des}} = \delta_{ail}$ then the integrator state is propagated using Equation 36.

B. Flight Path Angle Control

Vehicle flight path angle is controlled through the collective movement of the elevons, which will be called δ_{ele}. Flight path angle control is provided for two reasons. First, it allowes for the automatic adjustment of the nominal δ_{ele} trim to account for manufacturing tolerances. Second, it provides a guarantee that the vehicle is flying at the nominal flight speed. The desired flight path angle is computed from the desired L/D which is provided by the user. The flight path angle of the vehicle is computed using the vertical velocity and computed true airspeed from the navigation system.

$$\gamma_{cmd} = -\tan^{-1}\left(\frac{1}{L/D}\right) \tag{37}$$

The commanded flight path angle is computed using Equation 37 with the desired L/D for the vehicle to fly at. The value is negative, as the CICADA is a glider and will be descending. The actual flight path angle is computed using the true airspeed computed from Equation 7 and the estimated vertical velocity from Equation 6.

$$\gamma = -\sin^{-1}\left(\frac{V_D}{TAS}\right) \tag{38}$$

A proportional-integral controller is used to generate the desired elevator command.

$$e = \gamma_{cmd} - \gamma$$

$$\delta_{ele_{des}} = R_{p_{ele}}\left(e + x_\gamma\right) \tag{39}$$

$$x_\gamma = \int R_{i_{ele}} e \; dt \tag{40}$$

The desired elevator command from Equation 39 is limited to $\delta_{ele} = \text{sat}(\delta_{ele_{des}}, \pm\bar{\delta}_{ele})$ where $\bar{\delta}_{ele}$ is the maximum deflection allowed. If $\delta_{ele_{des}} = \delta_{ele}$ then the integrator state is propagated using Equation 40.

C. Control Surface Mixing

The flight control laws for roll and flight path angle generate roll and pitch axis commands in the form of δ_{ail} and δ_{ele}. These commands must be mixed to generate the final commands for the elevon control surfaces. Nominal trims are applied to the commands generated from the control loops.

$$\delta X = \delta_{ail} + \delta_{ail_{trim}} \tag{41}$$

$$\delta Y = \delta_{ele} + \delta_{ele_{trim}} \tag{42}$$

After the trims are applied the X-axis and Y-axis commands are mixed to generate the right wing servo command, S_R, and left wing servo command, S_L.

$$S_R = \delta X + \delta Y \tag{43}$$

$$S_L = -\delta X + \delta Y \tag{44}$$

Locking out the Y-axis command to allow the CICADA to safely fall away from the drop vehicle was found through flight testing. This was done by forcing the value δY to a nominal fixed value, δY^*, for a preset length of time. This timer was started when the hall-effect sensor is used to detected release of the CICADA.

D. Thermal Control

Because of the high altitude which the CICADA was designed to operate at it was required to provide battery heating. Lithium-polymer battery performance degrades quickly once the temperature drops below 0°-Celcius. The battery heater control was designed as a state machine with both temperature and voltage as an input. The inclusion of voltage in the control decision was based on the desire to prevent the heater from turning on if the battery voltage is already too low to sustain heater operation. A diagram of the heater control system is shown in Figure 4.

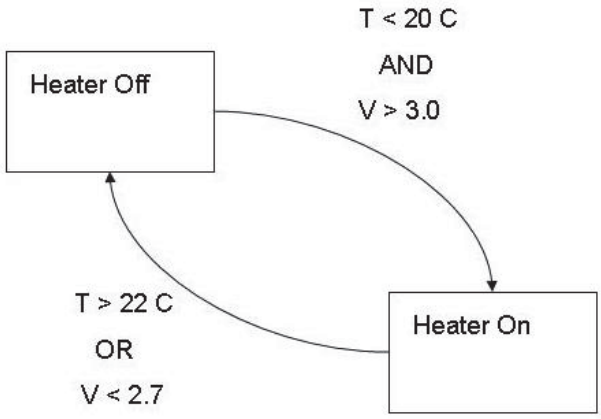

Figure 4: Battery heater control logic

VI. Flight Test

Flight testing of the CICADA began with a series of low-altitude drops. These tests were utilized to evaluate the performance and robustness of the flight control loops and navigation system to launch transients. Over 50 of these low-altitude drops were conducted. The next series of flight tests were performed from high altitude, culminating in drops from above 30,000 feet. These high altitude flight tests were used to validate the overall performance of the CICADA system, including the environmental controls, in a high altitude environment. Presented are sample results from a high altitude flight test showing the performance of the CICADA flight control system, and its ability to operate over a wide altitude range.

The high altitude flight tests were conducted at Yuma Proving Grounds in Arizona. A large helium-filled weather balloon was used to carry aloft a total of 3 aircraft, as shown in Figure 5a. A Tempest UAV mothership was used as the host platform for the CICADA vehicles. Figure 5b shows how two CICADAs were mounted on wing pylon drop mechanisms located on each wing of the Tempest. The Tempest was needed to carry the CICADAs back within range of the recovery site, as the balloon would drift with the prevailing winds too far downrange for the CICADAs glide back successfully.

During this test, the balloon carried the Tempest and CICADA combination to a maximum altitude of 57,000 feet above sea-level. At that point, Tempest was released from the balloon and automatically began to glide back towards the recovery site. At an altitude of 29,850 feet the first of the two CICADAs were released. Presented is the data from this particular flight, which is representative of all of the high altitude flights.

The horizontal projection of the flight path is shown in Figure 6a and the altitude profile of the flight is shown in Figure 6b. The performance of the guidance controllers can seen in Figure 6a. The straight line to the waypoint, located at the bottom of Figure 6a, is evidence that the track controller functioned perfectly. The orbit guidance controller performed adequately, keeping the vehicle in a tight orbit around the waypoint. The flight path angle controller performance can be seen in the straight altitude profile line and from the vertical velocity plot in Figure 7. The smoothness of the vertical velocity as shown in Figure 7 indicates the vertical velocity complementary filter is working correctly. The effect of altitude on the decent rate can also be seen. The variation of the vertical velocity shown the last part of Figure 7 is due to the periodic change in roll angle during the orbit. No feed-forward δ_{ele} was provided to account for the increased load-factor due to bank angle. The variation in ground speed in Figure 7 is due to wind.

The ground track and track error are shown in Figure 8. The performance of the track guidance controller is quite good, as seen in the track error shown in Figure 8b. The slight error in track during the orbit phase of flight is due to saturation of the roll axis as seen Figure 9.

Roll control response is shown in Figure 9. The roll attitude estimator was working well, as also evidenced by the near 0 roll attitude during the straight line segment of flight. It can also be seen that the roll controller was tracking the roll attitude commands from the guidance system. The maximum allowable roll was limited to ± 40 degrees.

(a) Balloon with Tempest UAV (b) Tempest UAV with CICADAs mounted

Figure 5: Balloon with Tempest and CICADAs and CICADAs mounted on Tempest UAV.

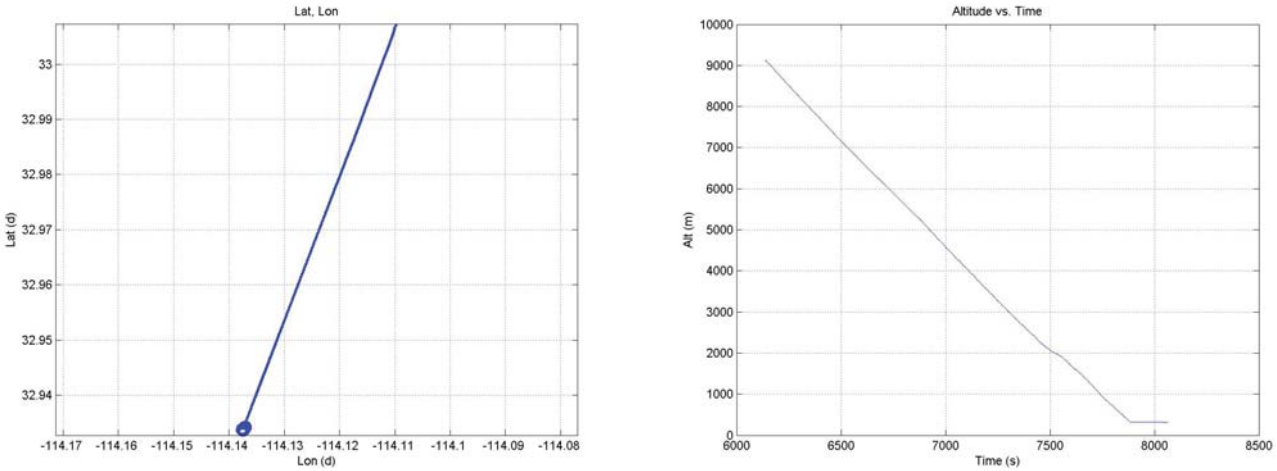

(a) Horizontal flight path (b) Altitude profile

Figure 6: CICADA flight path and altitude profile.

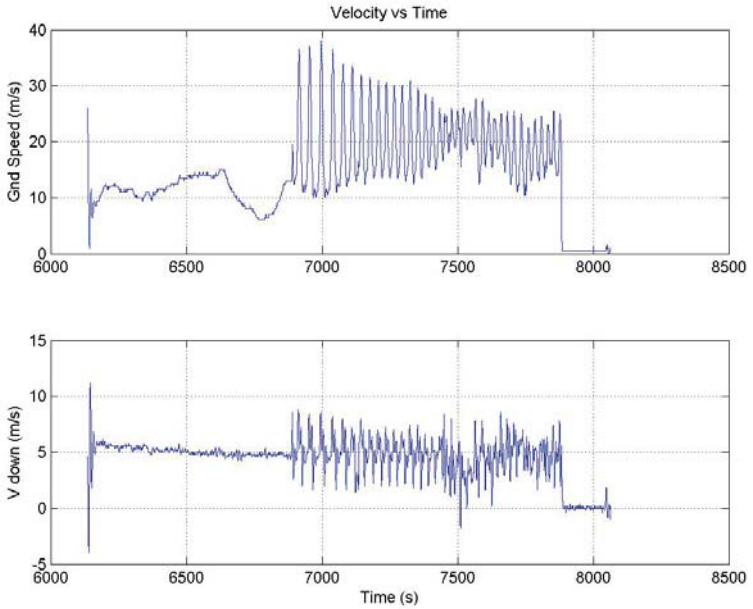

Figure 7: Velocity profile

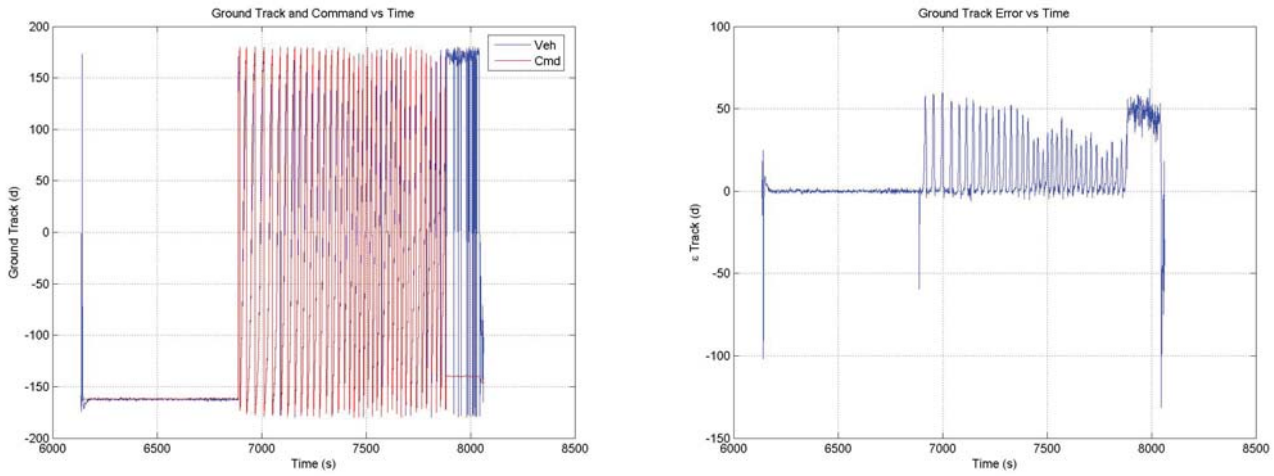

(a) Commanded and actual ground track

(b) Track error

Figure 8: CICADA ground track and track error

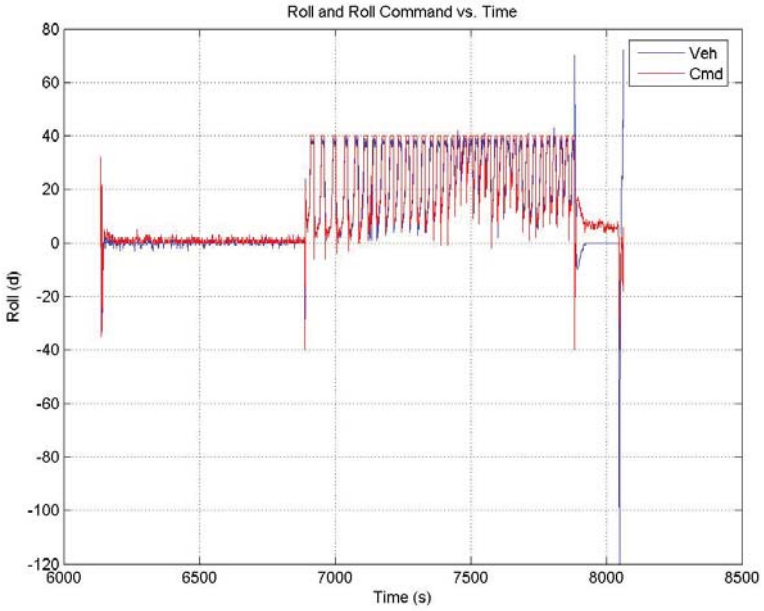

Figure 9: Roll control

The battery heater control loop was also functional in this flight, due to the cold temperatures at high altitude. The battery voltage during the flight stayed within acceptable bounds. Figure 10 illustrates the operation of the battery heater. It can be seen in Figure 10 that the heater was not able to maintain the battery temperature once the outside air temperature reached 0°-Celcius. This saturation of heater performance could be due to the drop of battery voltage during the long ascent to altitude under the balloon.

The performance of the wind and true airspeed estimation is shown in Figure 11. Based on the derivation of the wind estimator the wind is only fully observable during turning flight. During the long straight line flight towards the waypoint, the wind and true airspeed are not observable, resulting in incorrect data during this portion of the flight. Once the vehicle enters the orbit, these states become observable. After the flight, comparison of the the wind estimate and the observed winds fit well. Also, the true airspeed estimate matches well with the average ground speed shown in Figure 7 during the orbits.

The flight test data shows that the navigation, guidance, and control systems for the CICADA all performed correctly. The roll and flight path angle controllers tracked the commanded values well. The complementary filters for vertical velocity and roll attitude worked quite well as evidenced by the data.

VII. Conclusion

A new disposable air vehicle, CICADA, has been developed by the U.S. Naval Research Laboratory. This vehicle is capable of being dropped from a host platform from high altitude and automatically flying to a preprogrammed waypoint. The vehicle will orbit that waypoint until impact with the ground. The CICADA vehicle features a monolithic airframe/circuit board design with a minimal sensor suite. A robust navigation system was implemented to estimate roll attitude, vertical velocity, true airspeed, and north-east wind components. A basic guidance system was designed to command the vehicle towards the target waypoint and then orbit the waypoint precisely. Control loops for the regulation of roll and flight path angle were implemented using linear control theory. To help counter the negative affect of cold on the battery, a heater and thermostatic control loop was designed into the CICADA system. Flight test data from a drop of over 29,000 feet shows that the CICADA vehicle was successful in all aspects of the mission.

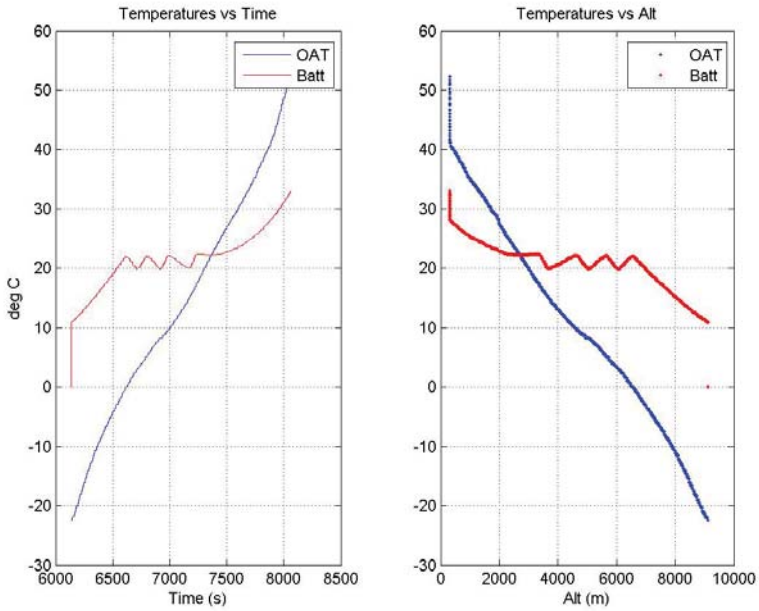

Figure 10: Battery heater operation

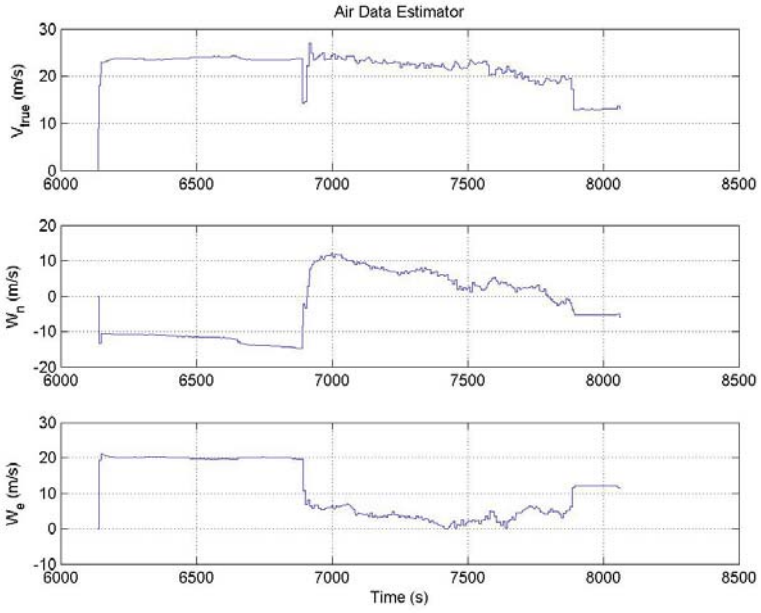

Figure 11: True airspeed and wind estimates

VIII. Thanks

Special thanks to Eric Peddicord for help with flight tests and environmental testing. Thanks to Chris Bovais and Steve Carruthers for assisting in making these flight tests possible. Final thanks goes to Mike Smith and AeroStar for their balloon support which made the high altitude testing possible.

References

[1]Kahn, A. D. and Foch, R. J., "High Packing Efficiency EAV for Local Area Seeding," *Joint Electronic Warfare Conference*, 2006.

[2]Johnson, E. N., Fontaine, S. G., and Kahn, A. D., "Minimum Complexity Uninhabited Air Vehicle Guidance And Flight Control System," *Proceedings of the 20th Digital Avionics Systems Conference*, 2001.

[3]Kahn, A. D. and Kellogg, J. C., "A Low-Cost, Minimum Complexity Altitude/Heading Hold Flight Control System," *21st Digital Avionics Systems Conference*, 2002.

[4]Taylor, B., Bil, C., and Watkins, S., "Horizon Sensing Attitude Stabilization: A VMC Autopilot," *Bristol UAV Conference*, Paper 22, 2003.

[5]Melexis, "MLX90247B Thermopile with On-Chip Thermistor," Tech. Rep. Rev 1.0, Feb 2001.

[6]uBlox, "u-Blox 6 Receiver Description," data sheet GPS.G6-SW-10018-A, apr 2011, http://www.ublox.com.

[7]STMicroelectronics, "LPY510AL: MEMS Motion Sensor," data sheet 15805 Rev 2, jul 2009, http://www.st.com.

[8]Semiconductors, N., "LPC213x User Manual," user manual UM10120 Rev 3, oct 2010.

[9]Stevens, B. L. and Lewis, F. L., *Aircraft Control and Simulation*, John Wiley and Sons, New York, 1992.

[10]Center, N. G. R., "Earth Atmosphere Model: Metric Units," Tech. rep., may 2011, http://www.grc.nasa.gov/www/k-12/airplane/atmosmet.html.

[11]Gelb, A., *Applied Optimal Estimation*, The MIT Press, Cambridge, Massachusetts, 1974.